frontiers | Frontiers in Marine Science

TYPE Original Research
PUBLISHED 12 September 2022
DOI 10.3389/fmars.2022.969461

OPEN ACCESS

EDITED BY
Selvaraj Kandasamy,
Xiamen University, China

REVIEWED BY
Xinxin Li,
Southern University of Science and Technology, China
Pei Sun Loh,
Zhejiang University, China

*CORRESPONDENCE
Shuqin Tao
taoshuqin@tio.org.cn
James T. Liu
james@mail.nsysu.edu.tw

SPECIALTY SECTION
This article was submitted to Marine Biogeochemistry, a section of the journal Frontiers in Marine Science

RECEIVED 15 June 2022
ACCEPTED 11 August 2022
PUBLISHED 12 September 2022

CITATION
Tao S, Liu JT, Wang A, Blattmann TM, Yang RJ, Lee J, Xu JJ, Li L, Ye X, Yin X and Wang L (2022) Deciphering organic matter distribution by source-specific biomarkers in the shallow Taiwan Strait from a source-to-sink perspective. *Front. Mar. Sci.* 9:969461. doi: 10.3389/fmars.2022.969461

Deciphering organic matter distribution by source-specific biomarkers in the shallow Taiwan Strait from a source-to-sink perspective

Shuqin Tao[1,2]*, James T. Liu[3]*, Aijun Wang[1,2,4], Thomas M. Blattmann[5], Rick J. Yang[3], Jay Lee[3], Jimmy J. Xu[3], Li Li[6], Xiang Ye[1,2], Xijie Yin[1] and Liang Wang[1,2]

[1]Third Institute of Oceanography, Ministry of Natural Resources, Xiamen, China, [2]Fujian Provincial Key Laboratory of Marine Physical and Geological Processes, Xiamen, China, [3]Department of Oceanography, Sun Yat-sen University, Kaohsiung, Taiwan, [4]Southern Marine Science and Engineering Guangdong Laboratory, Zhuhai, China, [5]Geological Institute, Eidgenössische Technische Hochschule (ETH) Zürich, Zürich, Switzerland, [6]Key Laboratory of Marine Chemistry Theory and Technology, Ministry of Education, Ocean University of China, Qingdao, China

Sedimentary organic matter (OM) in coastal systems is inherently diverse, often with multiple particulate sources and transport histories. The Taiwan Strait (TS) is a typical shallow conduit region, linking the East and South China Seas. Strong ocean currents, coastal upwellings, distal large rivers, and proximal small mountainous rivers all influence the distribution of OM in the TS. We investigated the covarying patterns in the distribution of gain size classes of sand, silt, and clay; terrestrial-sourced biomarkers (n-$C_{27+29+31}$ alkanes, n-$C_{26+28+30}$ fatty acids (FAs), and n-$C_{28+30+32}$ alkanols); marine-sourced biomarkers (phytoplankton-derived alkenones, brassicasterol, dinosterol, and zooplankton-derived cholesterol) in sea floor sediment; indicator satellite-derived primary production (Chl-a); and water-mass indicator (sea surface temperature, SST). We used an empirical orthogonal/eigen function (EOF) analysis to distinguish the influence of four hypothetical sources that entered the TS through the north, south, west, and east boundaries. Results show that input sources from the south-bound ZMCC (Zhejiang-Fujian Coastal Current) and north-bound SCSWC (South China Sea Warm Current) had the dominant influence on the OM distributions buried in the TS. Input sources via river plumes on lateral boundaries and upwellings in the TS were the secondary factors that affected the sedimentary OM distribution. Within this source-to-sink system of multiple sources and transport processes, silt and clay were the major carriers of the OM signals. Terrestrial biomarkers and primary production (Chl-a) were associated with the two major current systems and river plumes along the edge of TS. Marine biomarkers were associated with upwellings in the interior of the TS. Our finding points out that the physical systems of ocean

currents, river plumes, and upwelling not only determine the distributions of biomarkers in the TS but also determine the diversity of OM in the TS.

KEYWORDS

OM distribution, marine biomarkers, terrestrial biomarkers, Min-Zhe coastal current, South China Sea warm current, upwelling, fluvial input, the Taiwan Strait

1 Introduction

The Global Carbon Program (GCP) lists shelf marginal seas, terrestrial ecosystems, and oceans as three subsystems of the carbon cycle (Friedlingstein et al., 2019; Regnier et al., 2022). Burial of OM, a permanent carbon sink and natural "recorder" of the climatic and environmental changes for the marine and adjacent continental systems, marginal seas plays a significant role in the global and reginal biogeochemical cycles (Bianchi and Allison, 2009). Generally, marginal seas, influenced by heterogeneity in OM sources and complexity of transport processes, usually form a basin-specific diversity of OM distribution patterns (Blair and Aller, 2012; Bao et al., 2018b). For example, terrigenous and marine OM in refluxing deltaic fluidized muds at marginal seas influenced by large rivers, such as the Yangtze, Amazon, Mississippi, and Fly Rivers, with high sedimentation rates shows a lower range of burial efficiency from ~20% to 30% for terrigenous OM and 1.3% to 2.5% for marine OM, respectively (Burdige, 2005; Blair and Aller, 2012; Wu et al., 2013; Zhao et al., 2021). These types of continental margins often developed subaqueous delta slopes and mobile mud belts accompanied by high tidal energy, where the sediment depocenter can be moved farther off river mouths tens to hundreds of kilometers away (Walsh and Nittrouer, 2009). The mobile mud belt in the marginal sea system is commonly characterized by high suspension and just seems like an efficient "OM incinerator", which usually acts to enhance the degradation and lower the burial efficiency of both terrigenous and marine OM due to prolonged oxygen exposure time (Blair and Aller, 2012; Bao et al., 2018b; Zhao et al., 2021). Although a distal subaqueous clinoform system has also been formed by several cycles of transport, deposition, and resuspension under intense tidal, wave, and coastal conditions, burial efficiencies of terrestrial OM exported by the Yellow and Ganges-Brahmaputra Rivers are as high as 80% (Keil et al., 1997; Galy et al., 2007; Tao et al., 2016). Their high OM preservations are attributed to the refractory in nature and slow reactivity of exported terrigenous OM originated from Chinese loess deposit within the Yellow River drainage basin and the Himalayan uplands within the Ganges-Brahmaputra drainage basin, respectively (Galy et al., 2007; Galy and Eglinton, 2011; Tao et al., 2015; Tao et al., 2016). Due to the higher contribution of OM from petrogenic sources and the mechanism of rapid migration of terrigenous materials into the sea caused by short steep terrains and frequent extreme events (Kao et al., 2006; Hilton et al., 2008; Kao et al., 2014), small mountainous river dispersal systems have been identified as having the highest burial efficiency of OM (up to more than 90%) in spite of having moderate sedimentation rates by continental margin standards (Blair and Aller, 2012). Overall, the heterogeneity of sedimentary OM sources (e.g., fresh/refractory) and dispersal/sedimentary physical conditions (e.g., high/low energy) both control the nature and distribution of OM in marginal sea sediments. Besides, heterogeneous OM matrices and conceivably complex hydrodynamics and sedimentation processes in marginal seas may both lead to aliasing in organic geochemical proxies in sedimentary records (Xing et al., 2014; Tao et al., 2016; Bao et al., 2018a; Bao et al., 2018b; Bianchi et al., 2018; Coppola et al., 2018), which is challenging for tracking and inferring the source-to-sink pathways of OM of different origins in a temporal and spatial context here. Thus, it is essential to distinguish how the marine physical environment, and which intrinsic chemical nature, co-influences the sedimentary OM in order to obtain a more comprehensive understanding on OM source–sink behavior in marginal sea systems.

The TS is a narrow and shallow conduit linking two major Asian marginal seas with wide shelves dominated by distal Yangtze River and Pearl River fluvial sources. From the source-to-sink (S2S) perspective, this conduit is subject to seasonal monsoons and episodic deliveries of OM from several contrasting sources (Yang et al., 2021). Suspended particles exported from these rivers are transported by monsoon-regulated currents: the southbound ZMCC (Liu et al., 2021a) and the northbound South China SCSWC into the TS (Yang et al., 2021). ZMCC brings cold water mass and SCSWC brings warm water mass to the TS (Yang et al., 2021). Numerous small rivers on the western side (Zhejiang-Fujian Coast) and small mountainous rivers on the eastern side (Taiwan Coast) also contribute terrestrial materials into the TS *via* river plume dispersal (Milliman and Farnsworth, 2013; Lee et al., 2016; Liao et al., 2018). Additionally, there is evidence from the high correlations among the sea surface temperature (SST) and chlorophyll *a* (*Chl-a*) suggesting strong coupling between

physics and biology (Liu et al., 2019). Meanwhile, river plumes from both sides of the TS deliver terrestrial-sourced nutrients to the TS (Liu et al., 2019) which induced high *Chl-a* concentrations along the coasts on both sides of the TS. Coastal upwellings along the Zhejiang-Fujian coast and south of the Penghu Islands in the center of the TS also create ecosystems of high primary productivity and marine OM production (Liu et al., 2019). Thus, sources and compositions of sedimentary OM in TS are not only affected by land–sea interaction of the proximal area in the conduit, e.g., coastal upwellings and several fluvial inputs from the Taiwan and Min-Zhe coasts on both sides, but also from the two distal fluvial inputs from the world's major rivers (e.g., the Yangtze and Pearl Rivers). Thus, it is essential to fill in the knowledge gap regarding detailed distinction in the sedimentary OM distribution patterns and diversity in this complex conduit portion of source-to-sink sedimentary systems in marginal seas such as the TS.

The goal of this study is to distinguish terrestrial and marine biomarkers and establish their source-to-sink characteristics in the sea floor of the TS. Our dataset consists of three grain-size classes, three groups of terrestrial-sourced biomarkers, four marine-sourced biomarkers, satellite-derived *Chl-a*, and satellite-derived SST. We tested the influence of four hypothetical input sources using the EOF analysis technique to distinguish marine-derived from terrestrial-derived organic components and their distribution pathways in the TS and rank the validity of the hypothetical sources.

2 Material and methods

2.1 Study site and sample collection

The TS is a shallow and highly energetic coastal sea that links two major Asian marginal seas: the South China Sea and the East China Sea. The surface circulation of the TS consists of the northward flow of the extension of the SCSWC in the west and central parts, the northward flow of the Taiwan Warm Current (TWC) along the eastern part of the strait, and the southward flow of ZMCC (Figure 2). The deepest part of the TS is the Penghu Channel (PHC) in the southeast, which is the most important gateway through which the TWC as a Kuroshio Branch Current derived from the Luzon Strait flows into the TS. The Zhang-Yun Rise (ZYR) in the middle reaches of the TS is a topographic high impeding circulation between the Wu-Qiu Depression (WQD) in the southwest and the Guan-Yin Depression (GYD) in the northeast. The Taiwan Banks (TWB) in the southwest is a shallow and barren sand bank lying between the rest of the TS and the South China Sea (in the south) (Figure 1). On the west side, several medium–small-sized rivers such as the Min, Jiulong, and Han rivers export substantial sediments into the western TS. On the east side, many small mountainous rivers in Taiwan carry disproportionately high sediment yields (Figure 2). Previous studies have shown that fine-grained surficial sediment along the western TS coast tends to join the Zhe-Min mud belt derived from Yangtze River,

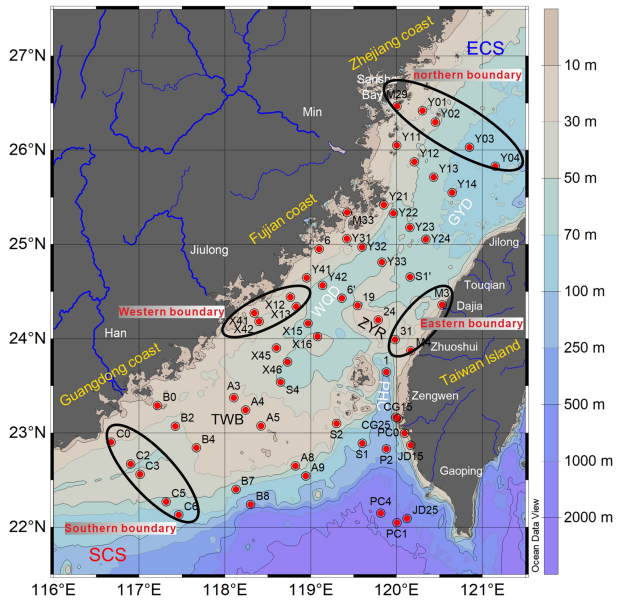

FIGURE 1
Surface sediment sampling sites (red dots) and designation of boundaries of water masses in the TS. TWB, Taiwan Banks; PHC, Penghu Channel; ZYR, Zhangyun Rise; GYD, Guanyin Depression; WQD, Wu Qiu Depression; ECS, East China Sea; SCS, South China Sea.

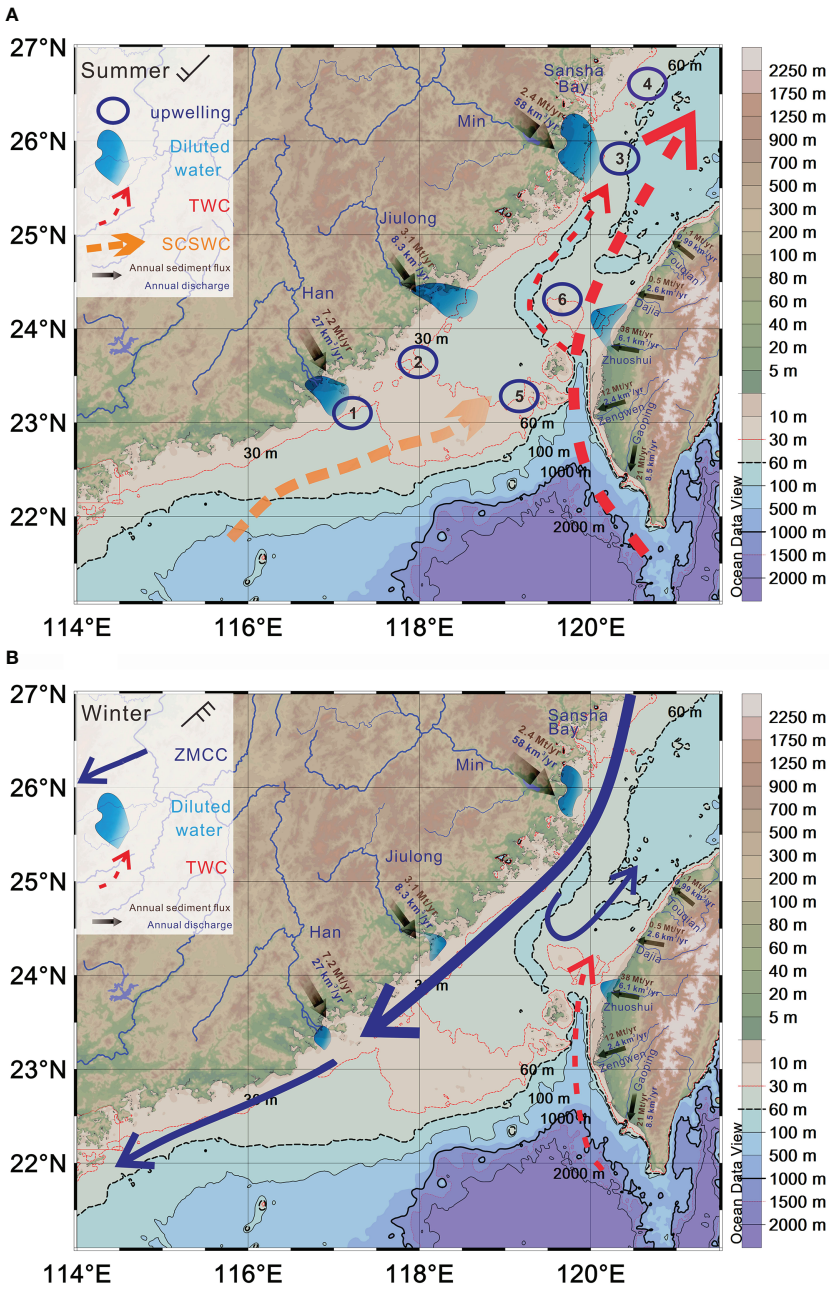

FIGURE 2
Seasonal circulation and its impact on sediment dispersion within the TS modified from Xu et al. (2009). Upwelling zones are defined by Liu et al. (2019). **(A)** In summer, small mountainous rivers from Taiwan discharge most of its annual sediment, the finer fraction being winnowed and transported northward by the energetic TWC and SCSWC. The dispersal of Zhuoshui River plume alternates alongshore controlled by the tide (Lee et al., 2016). **(B)** In winter, the remaining silts and sands mix with Yangtze clays that are transported southward by the ZMCC in winter. Annual discharges and sediment fluxes for individual rivers refer to Milliman and Farnsworth (2011).

whereas silt and sand along the middle and eastern TS originate from Taiwan Island (Xu et al., 2009; Huh et al., 2011; Liu et al., 2018). Recent studies point out a remote source for nutrients and suspended particles to the TS driven by the Pearl River estuarine plumes mixing with the SCSWC crossing the TWB and entering the TS in summer (Liu et al., 2019; Yang et al., 2021). The coastal upwelling usually occurs along the west coast triggered by the prevailing SW summer monsoon, which supplements nutrients

making the TS a region of high marine productivity (annual euphotic zone integrated value is 123 ± 86 g C m^{-2} $year^{-1}$; Tseng et al., 2020).

Surface (0–5cm) sediment samples (n = 62) covering the whole TS were collected in April 2016 on the R/V Yanping II and during 2012–2017 on the R/V Ocean Researcher I (OR1) (Figure 1 and Table S1). All samples were retrieved by a grab sampler and stored at −20°C prior to analysis. In the laboratory, sediment samples were lyophilized using an EYELA FDU-2100 Freeze Dryer, then homogeneously ground into powder with a mortar, and stored in a desiccator until analysis.

2.2 Satellite sea surface temperature and Chl-*a*

In order to provide water-mass and primary productivity information to constrain our data analysis, we employed the MODIS database of SST and *Chl-a* values derived from a satellite-born radiometer, using the annual mean SST and *Chl-a* from a 4×4-km grid averaged over 17 years from 2002 to 2019. With TS sedimentation rates ranging from 1 to 8 mm/year (Huh et al., 2011), our surface sediments (0–5 cm) would reflect conditions averaged over one to five decades. Thus, the 17-year average satellite annual SST and *Chl-a* should be comparable with those records in the surface sediments.

2.3 Bulk characteristic analysis

For grain-size analyses, 5 ml of 10% H_2O_2 was added to ~0.2 g of surface sediment sample at room temperature for 24 h to oxidize the OM. Then 1 ml of 3 mol/l HCl was added to the sample at room temperature for 24 h to remove any calcium carbonate. After centrifuging and decanting several times with Milli-Q water, samples were dispersed with 10 ml of 0.05 mol/l sodium hexametaphosphate solution and homogenized using ultrasound before passing through a Malvern laser diffraction grain sizer (Mayer, 1994; Keil et al., 1997). For bulk element content analyses, 5 ml of 2-M HCl solution was added to 1–2 g of surface sediment sample at room temperature for 24 h to remove the inorganic portion (mainly in the form of carbonate), and then acidified samples were rinsed, centrifuged and decanted five to seven times with Milli-Q water. Afterward, well-treated samples were then dried at 60°C and carefully crimp-sealed in tin capsules for element content (modified from Komada et al., 2008). Total organic carbon (TOC), total nitrogen (TN) content, and stable carbon isotope composition ($\delta^{13}C$) analyses were conducted on an elemental analyzer in the Stable Isotope Platform/Community Lab at the Third Institute of Oceanography, Ministry of Natural Resources of China. The precision for TOC content and $\delta^{13}C$ is better than ±0.2% and ±0.2‰, respectively.

2.4 Lipid biomarker analysis

In this study, our target lipid biomarkers include *n*-alkanes, *n*-alkanols, sterols, and *n*-fatty acid methyl esters (*n*-FAMEs). The methods for extraction, purification, and isolation of source-specific biomarkers were similar to those described by Tao et al. (2016). A total of 15 g of each freeze-dried and homogenized sediment sample was spiked with an appropriate amount of non-internal standard mixture (n-$C_{24}D_{50}$, n-C_{19} alkanol, and n-C_{19} fatty acid), then extracted with a mixture of dichloromethane (DCM) and methanol (MeOH) (3:1, v/v) four times *via* ultrasonication for 20 min. The resulting mixture was saponified with KOH/MeOH solution (6% w/w). Afterward, a "neutral" fraction and an "acid" fraction were backextracted from the hydrolyzed solution separately after adjusting the pH of solution. The "neutral" fraction was further separated by SiO_2 column chromatography into two fractions: the non-polar fraction eluted by 8 ml hexane containing n-alkanes and the polar fraction eluted by 12 ml DCM/MeOH (95:5, v/v) containing plant wax n-alkanols and marine phytoplankton sterols (brassicasterol, dinosterol and C_{37} alkenones). *n*-Alkanes were concentrated under N_2 to 60 μl with isooctane before measurements. *n*-Alkanols and sterols were derivatized using N, O-bis(trimethylsilyl)trifluoroacetamide (BSTFA) at 70°C for 1 h before measurements. The acid fraction containing the fatty acids (FAs) was transesterified to yield the corresponding fatty acid methyl esters (FAMEs) with a mixture of HCl/MeOH (5:95, 70°C for 12 h). The resulting FAMEs were further purified using SiO_2 column chromatography by elution with hexane/DCM (4:1, 4 ml) and then concentrated under N_2 to 100 μl with isooctane before instrumental measurements.

n-Alkyl lipid and sterol assignment was performed with thermo gas chromatography–mass spectrometry (GC–MS)and by comparison with the retention times of the standards. Quantification was performed with an Agilent 7890B GC instrument using an HP-1 column and He as carrier gas. The average relative standard deviation (%) was <10%.

2.5 The eigen function analysis

Because of the high visual resemblance nature of the measured variables, an EOF analysis was used to characterize the correlations (standardized covariability) of multiple variables in the TS. This technique is based on internal correlations (Resio and Hayden, 1975), which present the statistical characteristics

of a group of data through the spatial or temporal correlation of the data (Hong et al., 2009; Liu et al., 2019; Yang et al., 2021). Each eigenmode in the EOF result was ranked according to the quotient between the eigenvalue of the eigenmode and the sum of all the eigenvalues. The highest mode (mode 1) explains most of the covariability (correlation) in the data set, followed by mode 2, mode 3, etc. In this study, we examined 12 covarying variables independently measured in space of the TS, consisting of the following categories: three grain-size groups of the percentage content of sand, silt, and clay (Figures S1A–C); the content of terrestrial-sourced biomarkers including *n*-$C_{27+29+31}$ alkanes, *n*-$C_{26+28+30}$ FAs, and *n*-$C_{28+30+32}$ alkanols (Figures 4A, C, E); the content of marine-sourced biomarkers including phytoplankton-derived alkenones, brassicasterol, dinosterol and zooplankton-derived cholesterol (Figures 5A, C, E, G); water-mass indicator shown as 17-year averaged SST (Figure S2A); and primary producer indicator shown as 17-year averaged *Chl-a* (Figure S2B).

3 Results

3.1 Bulk characteristics

Bulk parameters for TS surface sediments are presented in Figure 3. Figures 3A, B show the spatial pattern variations of mean grain size (Mz) and sorting coefficient (σ_i) in surface sediments with the range from 0.4 to 7.4 φ and from 0.4 to 3.1 φ, respectively. Well-sorted sand-sized sediments (Mz = 0–4 φ, σ_i < 1 φ) are widespread in the southern part of the study area such as offshore of Guangdong, the TWB and the WQD, while poorly sorted mud (silt+clay, Mz = 5 z.bar; 8 φ, σ_i > 1.5 φ) occupies areas of the northwest along the Min-Zhe mud belt stretching from the mouth of the Yangtze River to near the Dajia River's mouth on the west coast of Taiwan. Surface sediments in the GYD, the middle of northern TS, and the southern Penghu Channel show a medium range of the mean grain size (Mz = 4–5 φ), suggesting typical silt characteristics.

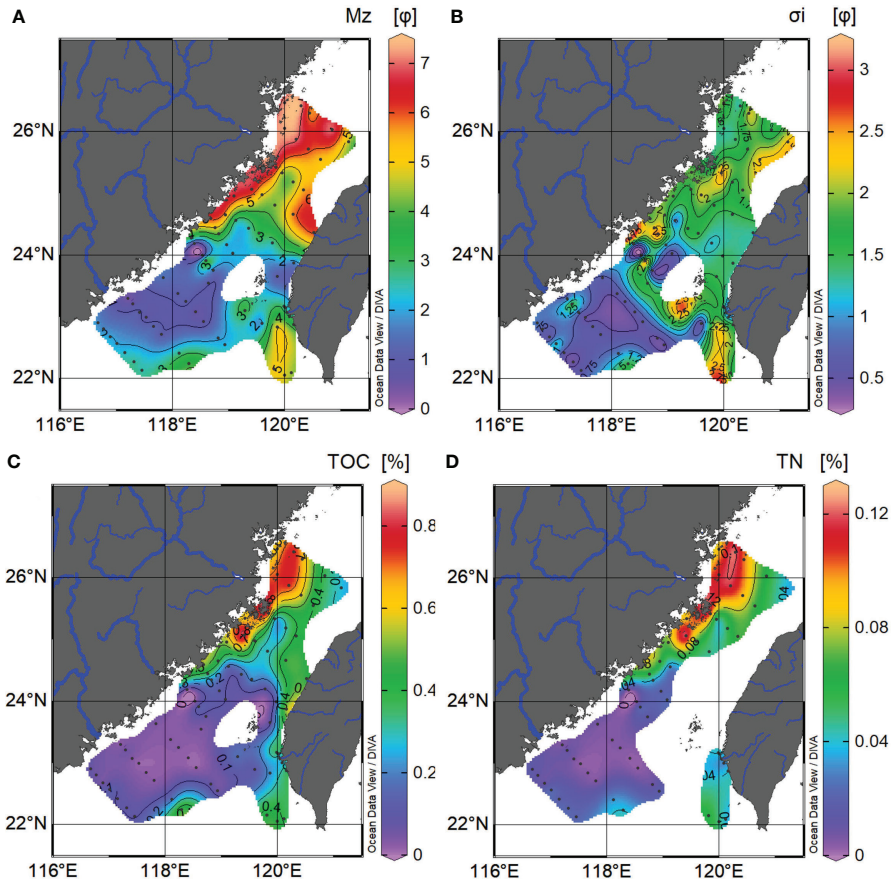

FIGURE 3
Spatial variations of grain size characteristics: **(A)** Mean grain size (Mz); **(B)** sorting coefficient (σ_i); **(C)** TOC content; and **(D)** TN content.

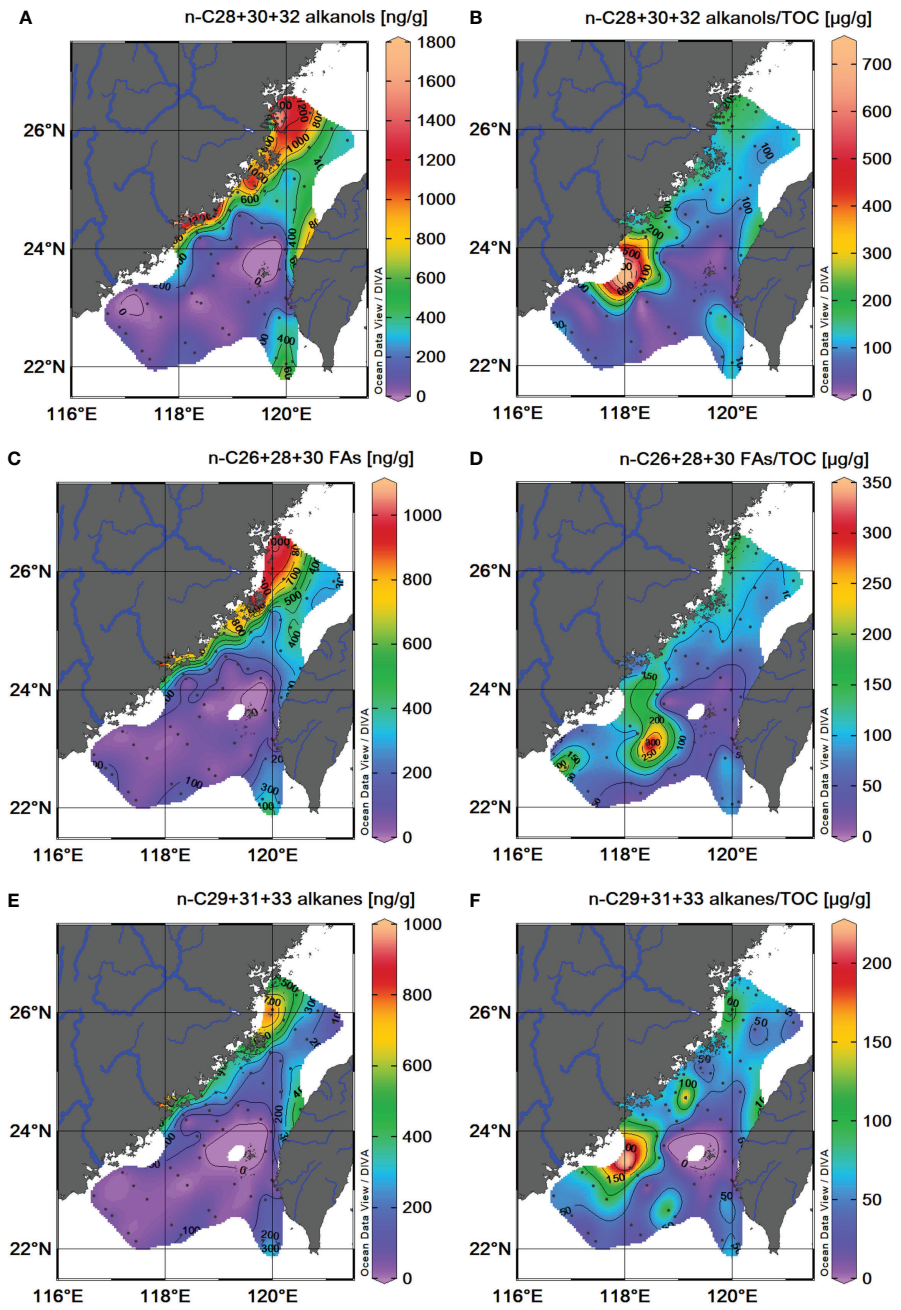

FIGURE 4
Spatial distributions of terrestrial biomarkers in TS surface sediments. Sediment dry weight and TOC-normalized n-$C_{28+30+32}$ alkanol content **(A, B)**; n-$C_{26+28+30}$ FA content **(C, D)**; n-$C_{27+29+31}$ alkane content **(E, F)**.

TOC and TN contents vary from 0.01% to 0.83% and from 0.003% to 0.12%, respectively, of which the spatial distribution generally decreases with distance off river mouths such as the offshore of the Min and Zhuoshui rivers (Figures 3C, D). TOC and TN contents display a statistically significant correlation and a positive, extremely low intercept (Figure S1, intercept = 0.002%, $R^2 = 0.96$, n = 59, $P < 0.001$), suggesting that TOC and TN come from the same origin and have less contributions from inorganic N sources in the study area. Besides, TOC and TN contents in the seafloor show the highest values along the northwest coast than those western TS and the lowest values in the TWB region (Figures 3C, D).

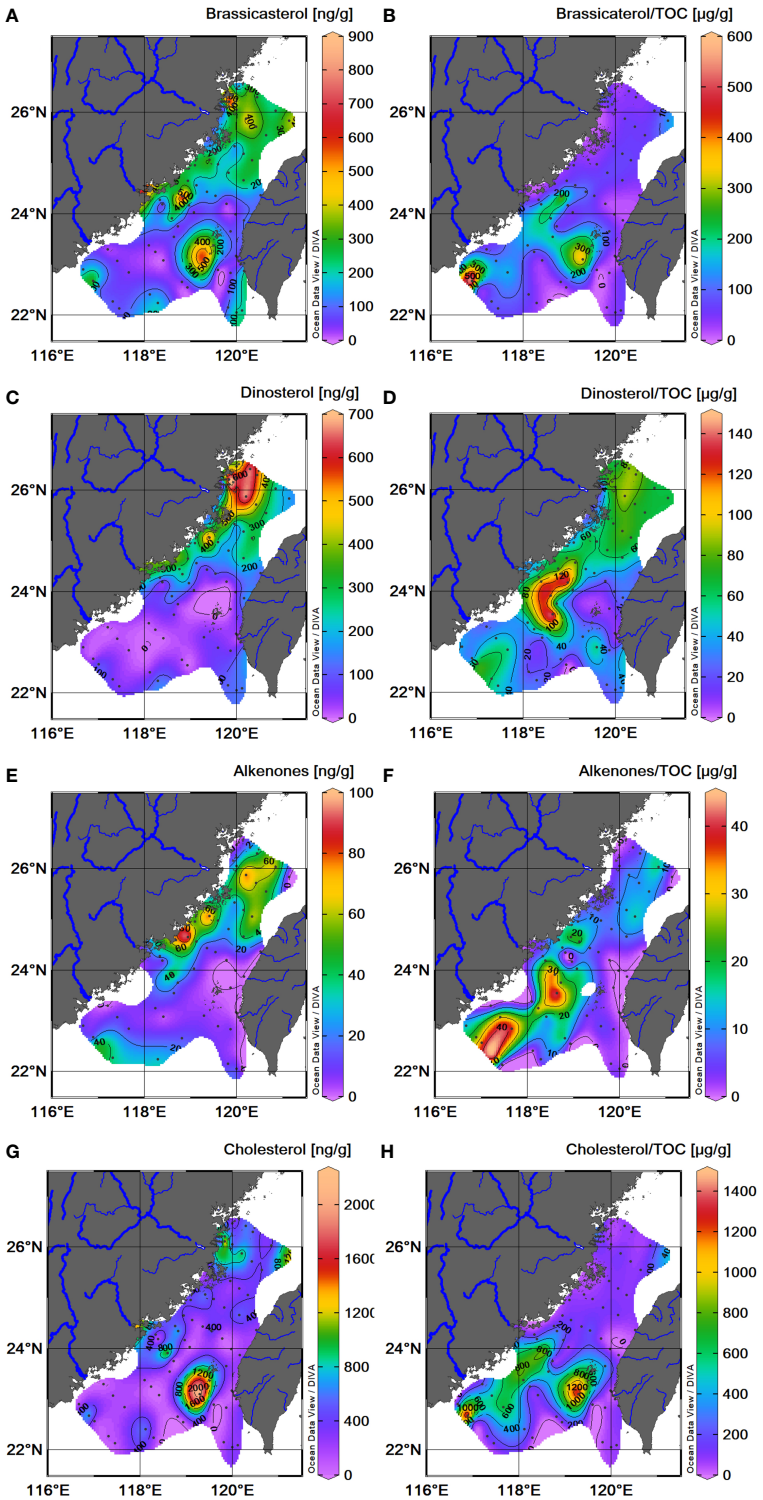

FIGURE 5
Spatial distributions of phytoplanktonic biomarker contents in TS surface sediments. Sediment dry weight and TOC-normalized brassicasterol content **(A, B)**; dinosterol content **(C, D)**; alkenones ($C_{37:2}$+ $C_{37:3}$) content **(E, F)**; cholesterol content **(G, H)**.

3.2 Lipid biomarker abundances

3.2.1 Terrestrial biomarkers

Even long-chain (n-$C_{28+30+32}$) alkanols, long-chain (n-$C_{26+28+30}$) FAs and odd long-chain (n-$C_{29+31+33}$) alkanes considered as terrestrial higher plant wax lipids have been widely used to track and infer the fate of terrestrial OM in the marine system (Eglinton and Hamilton, 1967; Eglinton et al., 2002; McDuffee et al., 2004; Rommerskirchen et al., 2006; Tao et al., 2016). The spatial distribution patterns of terrestrial biomarkers in surface sediments are mainly originated from fluvial material and significantly influenced by sedimentary and hydrodynamic conditions (Goñi et al., 1997; Weijers et al., 2009; Zhu et al., 2011a; Zhu et al., 2011b; Feng et al., 2013a; Feng et al., 2013b; Xing et al., 2014). Distribution patterns of dry weight of three groups of plant wax lipids in the surface sediment of the TS show an offshore decreasing trend away from the river mouths with a range from 4 to 1,217 ng/g (avg. 343 ± 355 ng/g), 7 to 1,001 ng/g (avg. 265 ± 278 ng/g), and 1 to 789 ng/g (avg. 166 ± 173 ng/g), respectively. The highest values were along the coastal region north of the Jiulong River on the western side of the TS and along the coastal region off Taiwan close to river mouths of the Zhuoshui and Dajia rivers on the eastern side (Figures 4A, C, E).

Regardless of OM sources, organic components have similar OM–particle interactions generally associated with benthic hydrodynamics and surface chemistry in sediments (Keil et al., 1994; Bao et al., 2018b). TOC-normalized source-specific biomarkers can offer better estimates of their origins to eliminate the influences of sediment environmental conditions (Xing et al., 2011; Mei et al., 2019). The TOC-normalized content of the above three plant wax lipids (n-$C_{28+30+32}$ alkanols, n-$C_{26+28+30}$ FAs, and n-$C_{29+31+33}$ alkanes) ranged from 12 to 701 μg/g TOC (avg. 111 ± 95 μg/g TOC), 10 to 313 μg/g TOC (avg. 87 ± 52 μg/g TOC), and 6 to 212 μg/g TOC (avg. 56 ± 37 μg/g TOC), respectively. Except the highest values at the northwest of the TWB, three groups of terrestrial biomarkers show higher TOC-normalized abundances along the coast region on both sides of the TS, especially near locations of river mouths (Figures 4B, D, F). Notably, a secondary value area of terrestrial-sourced FAs was in the southern TS south off Han River (Figure 4D).

3.2.2 Marine biomarkers

The sum of brassicasterol, dinosterol, and C_{37} alkenones has been widely used to track and infer the fate of marine-sourced OM in marine systems (Weijers et al., 2009; Li et al., 2014; Xing et al., 2014). These biomarkers are highly specific to diatoms, dinoflagellates, and coccolithophores, which are regarded as the dominant phytoplankton species in Chinese marginal seas (Feng et al., 2006; Zhou et al., 2015b). Generally, the contents of the three marine phytoplanktonic lipids (brassicasterol, dinosterol, and C_{37} alkenones) ranged from 5 to 684 ng/g (avg. 169 ± 137 ng/g), 0 to 683 ng/g (avg. 167 ± 175 ng/g), and 0 to 95 ng/g (avg. 24 ± 24 ng/g), respectively. They were higher in the west and north than those in the east and south of the TS. The higher values display a patchy distribution in the northwestern coastal areas and around Penghu Islands (Figures 5A, C, E). In addition, cholesterol in the marine sediment is commonly considered a synthesized product by marine secondary producers such as zooplanktons and other fauna (Grice et al., 1998; Bayona et al., 2002). Thus, the abundance of this lipid can reflect the fate of zooplankton-sourced OM in the marine system. The contents of cholesterol were higher in the offshore region ranging from 17 to 2178 ng/g (avg. 342 ± 340 ng/g), of which high values show a broadly similar patchy pattern to that of diatom-derived brassicasterol that occurred seaward of the river mouths along the northwestern coastal area and around Penghu Islands (Figures 5A, G).

The TOC-normalized content of three phytoplanktonic and zooplanktonic lipids mainly from marine origins ranged from 13 to 591 μg/g TOC (avg. 83 ± 91 μg/g TOC) for diatom-derived brassicasterol, 0 to 140 μg/g TOC (avg. 54 ± 31 μg/g TOC) for dinoflagellate-derived dinosterol, 0 to 41 μg/g TOC (avg. 10 ± 12 μg/g TOC) for coccolithophore-derived C_{37} alkenones, and 25 to 1,432 μg/g TOC (avg. 197 ± 273 μg/g TOC) for zooplankton-derived cholesterol, respectively. Three TOC-normalized phytoplankton-derived biomarkers show different patterns due to diverse ecological responses for each phytoplankton species. Diatom-derived brassicasterol and zooplankton-derived cholesterol show the highest values at upwelling regimes in the south part of the TS (Figures 5B, H), such as seaward of the Han River (#1, over the TWB (#2) and around the Penghu Islands (#5) as shown in Figure 2A. The consistency of spatial distribution between diatom-derived brassicasterol and zooplankton-derived cholesterol suggests the food–grazer relationship in the upwelling ecosystem. However, other typical upwelling areas offshore the mouth of the Min River and Sansha Bay in the northwestern coast (#3, #4) and around ZYR close to the Taiwan side (#6) had no corresponding higher proportions of diatom-derived biomarkers in sedimentary TOC (Figures 2A, 5B), which might be attributed to a large amount of terrestrial input (dilution effect) associated with ZMCC and local river input. Dinoflagellate-derived dinosterol shows higher proportions at offshore sites such as the WQD and southern and northern edges of the study domain (Figure 5D), where they are strongly influenced by intrusion of TWC, SCSWC, and ZMCC (Figure 2). Coccolithophore-derived C_{37} alkenones show the highest values at offshore sites in southern TS (Figure 5F), implying that coccolithophores in TS are more likely exotic species carried by intrusions of the warm SCSCC and the branched Kuroshio Current-TWC (Figure 2A).

3.3 Boundary of sediment input

For a broader regional view of the OM input associated with water masses in the study area, contour plots of the averaged satellite SST and *Chl-a* of 17-year-long records are as shown in Figure S2. They indicate the warm, oligotrophic northwestward-flowing SCSWC water that meets with the cold, eutrophic southeastward-flowing ZMCC, both driven by monsoon winds. Besides, the cold and eutrophic signal along the coastal region in the west TS can be also sustained by widespread coastal upwelling regions (Hong et al., 2009; Liu et al., 2019). Although the SST distribution over the TS does not show warm river plume signals, elevated *Chl-a* signals do occur at the mouth areas of the Min, Jiulong, Han, and Zhuoshui rivers (Figure S2), pointing to the influence over river plumes in material cycles including water mass, sediment, and their associated nutrients and OM. Thus, we hypnotized that physical systems of the ZMCC, SCSWC, southeast river plumes in the mainland (e.g., Jiulong and Han Rivers), and small mountainous rivers in Taiwan (e.g., the Zhuoshui and Dajia Rivers) could be important delivery systems for terrestrial-sourced OM. These systems enter the study domain through the boundaries at the north, south, east, and west of the TS (Figure 1).

3.4 Eigen function analysis

EOF analysis was used to examine the covariability among the 12 independent variables (three grain sizes, three terrestrial-sourced biomarkers, four marine-sourced biomarkers, satellite-derived *Chl-ai*, and SST) in five different versions of the dataset, including the raw data (without hypothetical source) and data specifying hypothetical sources from the north, south, west, and east boundaries (Figures S3 and 1). The strength/validity of each hypothesis is indicated by the accumulated percentages explained by the first two eigenmodes (Table 1).

Results showed that the 12 variables were by nature well correlated that the first two eigen modes combined explain 79.9% of the data covariability (Table 1). The validity of each hypothetical source is indicated by the percentage explained by the first two modes. Our findings show that OM distribution in the TS is influenced by the input from the four open boundaries at different degrees at the north, south, east, and west of the study domain (Figure 1). The input-specified deviation fields based on our hypotheses showed that the two longitudinal inputs from the north and south explained 90.4% and 85.1% of correlations, respectively. The two lateral hypothetical inputs resulted in 79.1% (from the west) and 80.2% (from the east), respectively (Table 1). The two hypothetical sources in the longitudinal direction (N-S) of the TS improved the data correlations, suggesting valid assumptions. This implies that the south-bound ZMCC and north-bound SCSWC were the dominant physical processes affecting the spatial distributions of the 12 variables. The two sources from the lateral boundaries (E-W) were not a strong hypothesis.

The eigen structures of the first mode of all deviation fields are robust, showing identical groupings (histograms in Figure 6 and Figure S3A) of all variables and their corresponding spatial patterns despite of the deviation fields (contoured eigenweightings). All variables except for sand and SST covaried in the positive group (Figure 6), including silt and clay, all biomarkers, and *Chl-a*. The corresponding spatial associations of these groups are weighted in the northern part of the TS which shows similar distribution patterns of measured clay, silt, and biomarkers (Figure 6). This indicates that clay and silt were carriers of terrestrial and marine biomarkers which were transported by the cold water in ZMCC having the influence of the Zhe-Min mud belt source. The negative group is weighted in the southern part of the TS, which was dominated by the distribution of sand (devoid of silt and clay) and the warm water mass (Figure 6), suggesting the influence of SCSWC and sandy TWB on sedimentary OM distribution at the south part of the study domain.

In mode 2, west- and east-sourced deviation fields are valid hypothetical sources such that they explain higher residual correlations (20.4% and 23.3%, respectively) than the longitudinal counterparts (5.1% and 8.6%, respectively) (Table 1 and Figure 7). Yet, the structures of eigenvectors and eigenweighting patterns of the north-sourced and south-sourced are still identical (Figures 7A, B). Under the influence of the two major current systems, the grouping by eigenvectors emphasized the plant-derived terrestrial biomarkers accompanied by *Chl-a* in the negative group and are weighted along the coast and near the river mouths shown in the contoured negative eigenweightings (Figures 7A, B). This suggests that higher primary biomass contributions indicated by *Chl-a* regardless of terrestrial and marine sources can be supported by proximal or distal fluvial input along with high levels of land-derived biospheric OM and

TABLE 1 The percentage explained by the first two eigenmodes of each deviation field.

%Correlation explained	Source unspecified	Sourced from north	Sourced from south	Sourced from mainland	Sourced from Taiwan
Mode 1	67.9	85.3	76.5	58.7	56.9
Mode 2	12.0	5.1	8.6	20.4	23.3
Sum	79.9	90.4	85.1	79.1	80.2

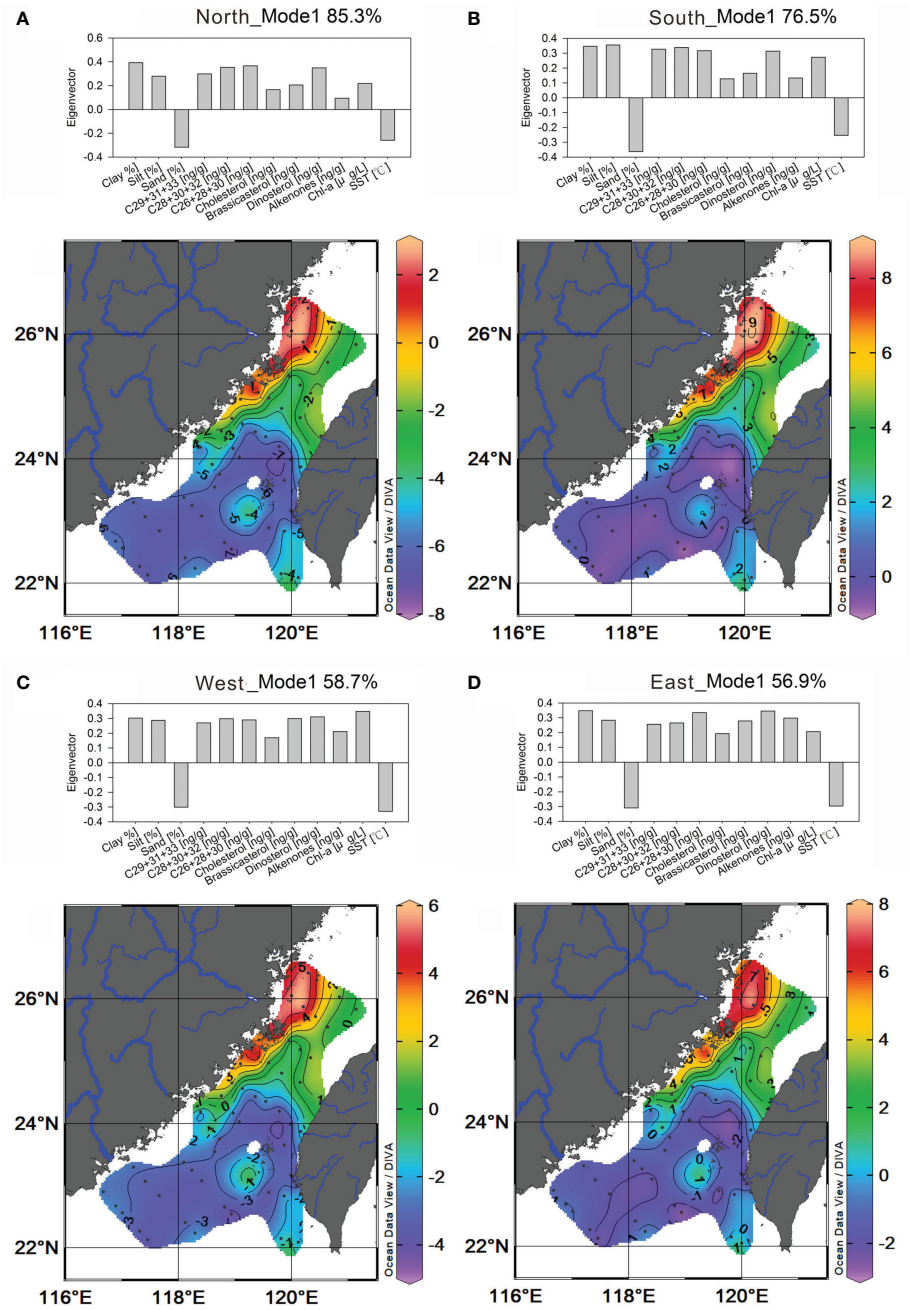

FIGURE 6
Plots of mode 1 eigenvectors (histograms) and contoured eigenweightings of the deviation field for hypothetical sources from the north **(A)**; the south **(B)**; west **(C)**; and east **(D)**.

nutrients. In contrast, eigenweightings of the four marine biomarkers (in positive values) are more localized, centered in the upwelling region south of the Penghu Islands (Figures 7A, B). Besides, two marine biomarkers strongly grouped in this mode and highly covaried in spatial patterns (R = 0.82, P <0.01; Table 2) including brassicasterol (diatom indicator) and cholesterol (zooplankton indicator) might suggest the food-grazing relation in the upwelling ecosystem.

Since there were no dominant physical processes in the lateral orientation, the first mode explains less correlation for the hypothetical sources from the west and east. Consequently, the second modes explain more residual correlations (20.4% and

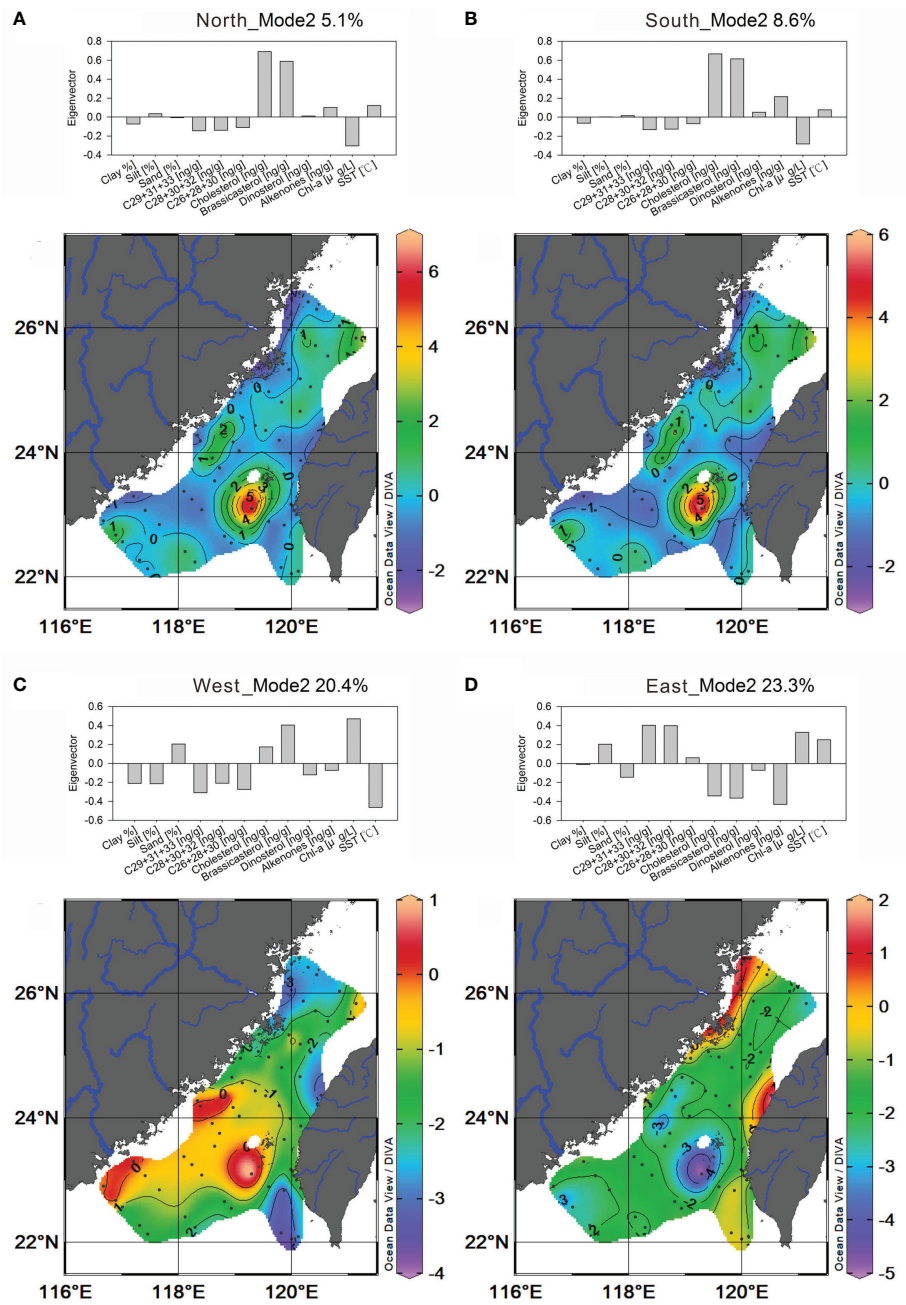

FIGURE 7
Plots of mode 2 eigenvectors (histograms) and contoured eigenweightings of the deviation field for hypothetical sources from the north **(A)**; the south **(B)**; west **(C)**; and east **(D)**.

23.3%) than the longitudinal counterparts (5.1% and 8.6%) (Table 1). Although the eigen structures of the west and east hypothetical sources are noticeably different, they do point to similar physical regimes with different OM and space associations (Figures 7C, D). The variables in the positive group of the west-sourced deviation field included sand, two marine biomarkers and *Chl-a*. The eigenweighting patterns of this group occupied southern TS with a broad filament extending northward (Figure 7C). Within this positive region, there are three high-valued areas which are located around Penghu Island and outside the mouths of Han and Jiulong Rivers near the coast. *Chl-a* and marine biomarkers are

TABLE 2 Cross-correlation coefficient (R) for the parameters of sedimentary properties, hydrological properties, TOC, and source-specific lipid biomarker contents in surface sediments from the TS.

Types of dataset	Parameters	TOC	*n*-$C_{29+31+33}$ alkanes	*n*-$C_{28+30+32}$ alkanols	*n*-$C_{26+28+30}$ FAs	Brassicasterol	Dinosterol	Alkenones	Cholesterol
Sedimentary properties	Clay%	**0.89****	**0.90****	**0.91****	**0.96****	0.55	**0.88****	0.49	0.35
	Silt%	**0.899****	**0.82****	**0.83****	**0.84****	0.58	**0.80****	0.61	0.35
	Sand%	**−0.89****	**−0.86****	**−0.87****	**−0.89****	−0.58	**−0.83****	−0.60	−0.35
	Sedimentation rate[a]	**0.789****	0.67	0.72*	**0.75****	0.54	0.71*	0.44	0.40
Hydrological properties	Annual SST	−0.38	−0.58	−0.583	−0.63	−0.41	−0.67	−0.57	−0.25
	Annual Chla	0.59	**0.68***	**0.7***	**0.71***	0.28	0.63	0.36	0.12
Bulk OM	TOC%		**0.86****	**0.90****	**0.92****	0.52	**0.87****	0.50	0.28
Terrestrial biomarkers	*n*-$C_{29+31+33}$ alkanes	**0.86****		**0.92****	**0.92****	0.46	**0.86****	0.48	0.25
	n-$C_{28+30+32}$ alkanols	**0.90****	**0.92****		**0.96****	0.50	**0.88****	0.47	0.28
	n-$C_{26+28+30}$ FAs	**0.92****	**0.92****	**0.96****		0.53	**0.92****	0.52	0.30
Marine phytoplanktonic biomarkers	Brassicasterol	0.52	0.46	0.50	0.53		0.63	0.54	**0.82****
	Dinosterol	**0.87****	**0.86****	**0.88****	**0.92****	0.63		0.65	0.37
	Alkenones	0.450	0.48	0.47	0.52	0.54	0.65		0.26
Marine zooplanktonic biomarkers	Cholesterol	0.28	0.25	0.28	0.30	**0.82****	0.37	0.26	

**Correlation is significant at the 0.01 level (2-tailed). *Correlation is significant at the 0.05 level (2-tailed). [a]Dataset of sedimentation rates are taken from the contoured map of ^{210}Pb-derived linear sedimentation presented in Huh et al. (2011). High correlation coefficients are highlighted by the bold.

associated with cold water (opposite to SST) (Figure 7C), suggesting the effect of upwelling (high marine primary production but low SST). The variables in the negative group are clay, silt, most terrestrial biomarkers, and SST (Figure 7C), which are weighted along the coasts of the TS, suggesting enhanced warm river plume effluent separated by the positively weighted area.

In the east-sourced deviation, marine biomarkers were in the negative group that occupied similar regions as the positive group of the west-sourced deviation (Figures 7C, D). The marine-sourced negative group is opposite to SST, also suggesting the influence of cold water, and its effect enhanced at the upwelling region in the contoured negative eigenweightings (Figure 7D). However, in this deviation field, the variables in the positive group included silt, terrestrial biomarkers, SST and *Chl-a*. The eigenweighting patterns of this positive group are weighted along the coasts in northern and central TS (Figure 7D). In addition, these three high-valued areas are located at the mouths of the Min, Zhuoshui, and Dajia rivers and the Gaoping Shelf-Canyon (Figure 7D). Terrestrial biomarkers, *Chl-a*, and SST are in the same group, suggesting the effect of river plume (i.e., high temperature associated with high primary productivity and land-derived material supplies). In the eastern-sourced deviation, eigen structures emphasized the TS-wide distribution of terrestrial biomarkers from rivers from both sides of the TS, whereas the western-sourced deviation emphasized the TS-wide distribution of marine biomarkers originated from upwellings.

4 Discussion

4.1 Physical systems have the primary control of source-specific biomarker distributions

Our EOF analysis showed that among four hypothetical sources, the north- and south-sourced inputs improved the data correlation (Table 1), and there is no difference in the mode 1 eigen structure. The contoured eigenweighting of mode 1 for the five deviation fields display a north–south partition in the TS, reflecting identical spatial patterns with the clay content (Figures 6 and S1A). Thus, mode 1 clearly represents a dominant controlling factor of surface chemistry or the particle affinity effect on patterns of the sedimentary OM distributions. Within this pattern, all the biomarkers and associated OM are carried by silt and clay and were associated with ZMCC. In the TS, clay- and silt-sized sediments are generally derived from input such as the southern end of the Zhe-Min mud belt that is carried by the ZMCC sourced from Yangtze River and minorly derived from medium-sized or small mountainous rivers on both sides of the TS (Huh et al., 2011; Xu et al., 2012; Chen et al., 2016). Coarse sediments are generally derived from sandy TWB and cross-shelf delivery by the SCSWC and result in a low level of sedimentary OM distribution at the southern part regardless of terrestrial and marine OM in the TS seafloor. The *n*-$C_{29+31+33}$ alkanes, *n*-$C_{28+30+32}$ alkanols, and *n*-

$C_{26+28+30}$ FAs mostly derive from higher plant leaf waxes and thus serve as tracers of terrestrial vascular plant OM (Eglinton and Hamilton, 1967). Contents of these long-chain plant wax lipids, dinoflagellate-originated dinosterol, and sedimentary TOC, each covarying strongly with sedimentary properties (e.g., grain size and sedimentation rates) in the spatial pattern, show a highly positive/negative correlation with spatial variations of fine-/coarse-particle sedimentation (all cross-correlation R >|0.80|, $P < 0.01$, Table 2). This implies that the content of terrestrial biomarkers and associated OM is controlled by the overall sediment flux and particle affinity, which in turn is influenced by natural and anthropogenic impacts on the adjacent fluvial dispersal systems (Liu et al., 2008; Xu et al., 2012). For the other three marine-sourced biomarkers, the spatial distribution of diatom-sourced brassicasterol, coccolithophore-sourced C_{37} alkenones, and zooplankton-sourced cholesterol also shows a weak positive/negative correlation with fine-/coarse-particle sedimentation (all cross-correlation |0.35| < R <|0.61|, Table 2). This implies that the content of marine biomarkers and associated OM is only at a certain degree controlled by the overall sediment flux and particle affinity, but OM provenance considerably affects the distribution of marine-sourced biomarkers, which in turn is influenced by regional marine primary production supported by the adjacent eutrophic river plumes and the upwelling processes (Liu et al., 2019). As one of typical marine phytoplanktonic biomarkers in marginal sea systems, the distribution of dinoflagellate-sourced dinosterol in the TS seafloor shows analogous traits as the three terrestrial biomarkers, which show higher contents where fine particles are deposited along the southern distal of the Min-Zhe mud belt (Figure 5C). This implies that dinoflagellate-produced OM buried in the TS shows the same behavior as the terrestrial materials during the pre-deposition histories, which is also consistent with a massive dinoflagellate algal bloom breakout in the Yangtze River estuary and its adjacent shelf (Zhang et al., 2015) and a high density of dinoflagellate cysts commonly buried in muddy sediments (Dale, 1976; Yamaguchi et al., 2002; Liu et al., 2021b). Therefore, better preservation in muddy sediments should be attributed to high abundances of dinoflagellate cysts and associated OM.

Besides, tidal currents play an important role in the hydrodynamics as well as sedimentation dynamics in estuarine, coastal, and shelf environments. The resuspension process is a ubiquitous phenomenon in the marginal sea systems due to the strong tidal current impact. In the TS case, a typical strong-current-high-energy-system (SCHES) by tide influenced by two distal fluvial systems (the Yangtze and Pearl Rivers) can cause an intensive vertical disturbance and resuspension on the water bodies or near-surface sediments especially for the shallow TS conduit (Wang et al., 2003; Yang et al., 2021), which result in 65%–85% of suspended particulate matter derived from bottom sediment to interfere with OM burial and enhance sedimentary OM remineralization with a poor TOC content (0.01% to 0.83%) (Wang et al., 2017; Wang et al., 2018). On the contrary, the Yellow Sea (YS) case—a typical weak-current-low-energy-system (WCLES) by tide—is influenced by a distal large river (the Yellow River) dispersal system. The combined effect of a weak tidal current and a "water barrier" formed by the coastal current and the Yellow Sea Warm Current makes a relatively stable deposition environment especially for the center mud region of the southern YS (Zhou et al., 2015a; Gao et al., 2016), which is characterized by sedimentary convergence and a low energetic seafloor to promote OM burial with a higher TOC content signal (0.5% to 1.28%) (Bao et al., 2016; Tao et al., 2016).

Thus, the physiographic setting determines the distribution patterns of different-sourced OM in the TS. Hypothetical input sources from the south-bound ZMCC and north-bound SCSWC had the dominant influence on the OM distributions in the TS. Input sources *via* river plumes on lateral boundaries and upwellings were the secondary factors that affected the OM. Within this source-to-sink system of multiple sources and transport processes, silt and clay were the major carriers of the OM signals in a high-energy-level conduit system such as the TS. In summary, the spatial distribution patterns of terrestrial and marine biomarkers in surface sediments are separately originated from fluvial material and *in situ* marine productions, both of which are strongly influenced by particle grain size which in turn is regulated by local sedimentary or hydrodynamic conditions during transportation and deposition (Xu et al., 2009; Huh et al., 2011; Xu et al., 2012; Liu et al., 2018).

4.2 Physical systems generate diverse source-specific OM in the TS

The eigen structures of the second eigen mode further distinguished the longitudinal transport of hypothetical sources from the lateral transport of hypothetical sources (Figure 7). Four deviation fields in mode 2 suggest that different physical systems generate diverse source-specific OM in the TS. The ZMCC system which dominated in the north boundary has brought a high level of land-derived biospheric OM (Figures 4A, C, E) and nutrients derived from the Yangtze River, thus contributing to local fisheries along the northwest part of coastal regions in the TS (Lan et al., 2014; Lan et al., 2017).

Widespread upwellings of the western TS are associated with the prevailing southwest monsoon winds parallel to the coast that induces seaward Ekman transport at the surface. Upwelling cools and injects nutrients into the upper water, thus supporting local marine OM productions (Hu et al., 2001; Hong et al., 2009). Meanwhile, the eigenweighting pattern of west-sourced deviation fields which dominated in mode 2 shows a similar spatial pattern with TOC-normalized diatom and zooplankton-sourced lipid content in surface sediments (Figures 5B, H, 7C).

Thus, it implies that the cold and nutrient-rich upwelling systems generate marine OM input within the basin, such as typical upwelling regimes outside the mouth of Han (#1), Jiulong Rivers and over the TWB (#2), and around Penghu Islands (#5) (Figure 2A). However, the typical high primary production in the upper water column associated with nutrient-rich coastal upwelling areas offshore from the mouth of the Min River (#3) and Sansha Bay (#4) had no corresponding higher eigenweighting values in the west-sourced deviation field, which can be attributed to the dilution effect of ZMCC in transporting terrestrial OM carried by silt and clay highlighted by the negative group in the north part of the study domain (Figure 7C).

In addition, the rivers on the two sides of the TS (Min River, Jiulong River, Han River on the mainland side, and small mountainous rivers on Taiwan side; Figure 1) provide warm freshwater and abundant land-derived nutrients into the TS. High primary production is also sustained by land-derived nutrients delivered to the coastal region by river plumes in the TS (Wu et al., 2017; Liu et al., 2019; Yang et al., 2021). Due to the lack of upwelling system distributed in the east coast of the TS, the east-hypothetical sources dominated in mode 2 clearly constrained the warm river plume with high land-derived nutrients generating terrestrial-sourced OM input within the basin. Three areas of high eigenweighting value of the east-sourced deviation field (Figure 7D) are consistent with high abundance patterns of three terrestrial biomarkers (Figure 4). This implies that terrestrial-sourced OM input, delivered by relatively warm river plume, is strong near the mouth of the Min River and small mountainous rivers on the Taiwan side. Low abundances in sediments and highest proportions in TOC for terrestrial biomarkers in the northwestern TWB can be explained by large amounts of well-sorted residual sands mainly from deltaic, coastal, and eolian origin (Cai et al., 1992), in which parts of refractory terrestrial OM can survive in these high-energy settings.

In order to constrain the interpretations of controlling factors' impact on the spatial distributions of source-specific biomarkers and their associated OM in the sea floor of the TS based on the above EOF analysis, bulk $\delta^{13}C$ and C/N ratios have been applied to give a hint of diverse origins of sedimentary OM (Figure 8). Due to the extremely low nitrogen content for coarser sandy sediments which are widely distributed in the eastern TS sea floor, C/N ratios are absent and invalid for the OM source indicator (Figure 8B). Higher C/N ratios (9.9 to 11.8) and relatively depleted $\delta^{13}C$ values (−23.8‰ to −25.3‰) generally occurred near the river mouths (e.g., Min, Jiulong and western Taiwan Island small mountainous rivers), suggesting a distinct C_3 terrestrial biospheric OM buried near the river mouths through lateral fluvial processes from both sides of the TS. Although strong ZMCC and river plumes indeed carried a substantial amount of fluvial materials as well as terrigenous OM from the distal Yangtze River and small southeast rivers on the Zhejiang-Fujian coast into the TS (Xu et al., 2012), high primary production can cancel off or dilute geochemical signals from terrestrial OM in the outer estuaries and coastal regions in the western TS, which is marked by high marine biomarker, nutrient, and Chl-*a* concentrations triggered by widely developed coastal upwelling regimes and river plumes (Liu et al., 2019; Lan et al., 2020; Tseng et al., 2020). Moderate C/N and $\delta^{13}C$ signals (7.0 to 8.0 and −21.5‰ to −22.5‰, respectively) appear alongshore at the west TS coast, indicating a mixture of marine and terrestrial OM derived from the Zhe-Min mud belt as the distal part of the Yangtze River material (Liu et al., 2018). The lower C/N ratios (5.0 to 7.0) and higher $\delta^{13}C$ values (−20.8‰ to −21.0‰) are shown at the southern TS such as TWB, offshore outside the southeast river mouths of the Han and Jiulong, the southwest region of the Penghu Islands, and the relatively deep region southeast of the TWB, indicating an enhanced marine OM contribution at the offshore region.

A plot of the bulk C/N ratio *versus* $\delta^{13}C$ has been used to constrain OM sources in the TS (Figure S4). These two geochemical characteristics of bulk OM range from −20.8‰ to −25.3‰ for $\delta^{13}C$ and 4.8–11.8 for C/N ratios, which overlaps with values expected from the mixture of terrestrial C_3 pedogenic OM originated from the southern China mainland and western Taiwan Island ($\delta^{13}C$ = −27.6‰ ± 1.5‰; C/N = 10–100; Kao and Liu, 2000; Hilton et al., 2008; Hilton et al., 2010), sedimentary rock-derived OM ($\delta^{13}C$ = −24.8 ± 2.0‰, C/N = 5.5 ± 1.3; Hilton et al., 2010), and marine biomass-derived OM ($\delta^{13}C$ = −19‰ to −22‰; C/N = 4–7; Fry and Sherr, 1989; Hedges et al., 1997). In the western TS, sample points (red dots) are falling on the mixing line between marine and terrestrial biospheric OM sources, indicating a dominant two-endmember mixing pattern of marine and terrestrial C_3-derived OM with the absence or limitation of sedimentary rock-derived OM contribution. The depleted $\delta^{13}C$ and higher C/N signals are trapped at the inner part of Chinese mainland southeast river mouths on the west side (Figure 8), also confirming that the lateral input of Chinese-mainland southeast rivers from the west of the study domain is a minor input for sedimentary OM over the TS. High-nutrient river plumes along with strong coastal upwelling systems trigger a large amount of marine primary production export (Wu et al., 2017; Liu et al., 2019; Yang et al., 2021). The western TS performs higher $\delta^{13}C_{TOC}$ values and lower C/N ratios of sedimentary OM than their counterparts in the eastern TS (Figure 8), indicating significant ^{13}C-enriched marine OM additions. This is also consistent with the results derived from the western-sourced deviation analysis (Figure 7C) and implies a TS-wide distribution of marine biomarkers originated from upwelling processes, especially near the west coast of the TS.

In contrast, sample points located at the TWB (yellow dots), center (orange dots), and eastern TS (blue dots) are falling under

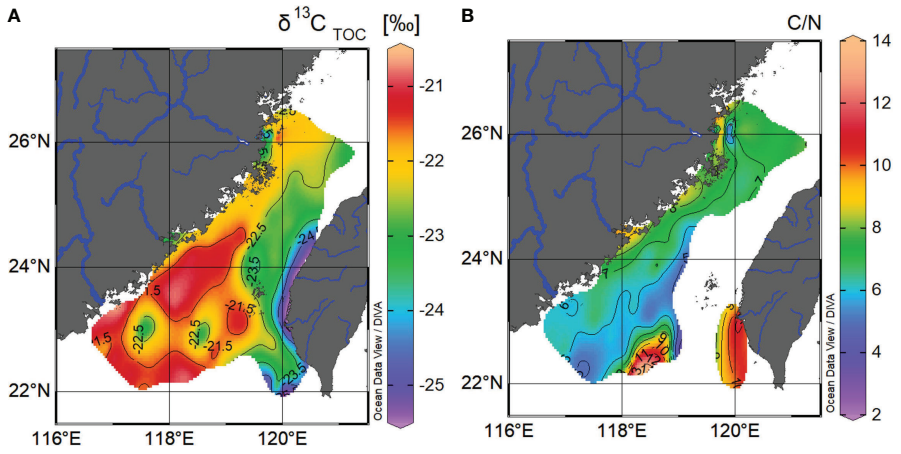

FIGURE 8
Spatial distributions of $\delta^{13}C_{TOC}$ **(A)** and C/N ratio **(B)** in the TS surface sediments. One data point within the Jiulong estuary (117.784°E, 24.481°N) and the averaged signal calculated from 31 surface sediments within the Min estuary are included in order to constrain Chinese mainland-derived fluvial OM origins into the TS from the west side.

the mixing line between marine and terrestrial biospheric OM sources (Figure S4), suggesting that at least another moderately ^{13}C-depleted and low C/N-derived OM was poured to and then buried in the TS. Sedimentary rock-derived OM could be a plausible origin, which has been reported to originate from the upland rock erosion or chemical weathering through the Taiwan-side mountainous fluvial or cross-shelf transport processes (Hilton et al., 2008; Kao et al., 2008; Zheng et al., 2017). In the eastern TS, the extension of depleted $\delta^{13}C$ and higher C/N tongue stretching from river mouths indicates that significant terrigenous OM from small mountainous rivers on the Taiwan side can escape from the river mouths and reach the center of the TS. An episodic and pulse delivery of sediment *via* small mountainous rivers on the east side leads to enhanced terrigenous material transferred further and buried rapidly (Kao and Milliman, 2008; Liu et al., 2008; Blair and Aller, 2012; Liu et al., 2013). However, the strong currents of the TWC and SCSWC pass through the center TS (Figure 2A) and push these fluvial OM northward into the East China Sea (Kao et al., 2008; Huh et al., 2011). Therefore, the influence of small mountain rivers from the east side is blocked to the eastern and central TS.

5 Conclusions

In summary, clay and silt are effective carriers of both marine and terrestrial biomarkers which are often associated with *Chl-a*. The two marine biomarkers are more weighted in the upwelling region, which show a food-grazing connection. The two current systems, ZMCC and SCSWC, are the major drivers for the longitudinal distributions of the OM in the TS. Minor drivers are the lateral fluvial inputs from both sides of the TS by river plumes and upwelling processes. Terrestrial biomarkers and primary production (*Chl-a*) were associated with the two major current systems and river plumes along the edge of TS. Marine biomarkers and associated OM were associated with upwellings in the interior of the TS. Our finding points out that the physical systems of ocean currents, river plumes, and upwelling not only determine the distributions of biomarkers in the TS but also determine the behavior of diverse-sourced OM buried in the TS. Meanwhile, EOF is an effective tool to extract information out of the complex dataset, which was otherwise hard to decipher.

Data availability statement

The original contributions presented in the study are included in the article/Supplementary Material. Further inquiries can be directed to the corresponding authors.

Author contributions

ST conceived and designed the study, supervised the work, and drafted the manuscript. JTL carried out the EOF analysis and related interpretation and cowrote the manuscript. AW contributed to the sediment collection and data interpretation and cowrote the manuscript. TB contributed to the cowriting of the manuscript and language polishing. RY, JL, and JX participated in the sediment collection, grain size analyses and the data plotting. XY, LL, and XJY contributed sample analyses on organic geochemical measurements. LW contributed to part

of the grain size measurements. All authors contributed to the article and approved the submitted version.

Funding

This study was supported by the National Key Research and Development Program of China (Grant No. 2019YFE0124700), Natural Science Foundation of Fujian Province (2020J05076), Xiamen Youth Innovation Fund Project (Grant No. 3502Z20206097), Scientific Research Foundation of Third Institute of Oceanography, MNR (Grant Nos. 2019018 and 2017013), National Natural Science Foundation of China (Grant Nos. 41506089, 41776099, and 41961144022), National Programme on Global Change and Air-Sea Interaction of China (GASI-04-HYDZ-02) and Innovation Group Project of Southern Marine Science and Engineering Guangdong Laboratory (Zhuhai) (No. 311021004). Data and samples were collected onboard R/V Yanping II implementing the open research cruise NORC2016-04 supported by the NSFC Shiptime Sharing Project (No. 41549904).

Acknowledgments

We would like to thank Ms. Liping Jiao and her student at the TIO for assisting sediment pretreatments, and Prof. Chin-Chang Hung from the National Sun Yat-sen University, Kaohsiung, Taiwan, for providing sediment samples of the southeastern TS.

Conflict of interest

The authors declare that the research was conducted in the absence of any commercial or financial relationships that could be construed as a potential conflict of interest.

Publisher's note

Supplementary material

The Supplementary Material for this article can be found online at: https://www.frontiersin.org/articles/10.3389/fmars.2022.969461/full#supplementary-material

References

Bao, R., Mcintyre, C., Zhao, M., Zhu, C., Kao, S. J., and Eglinton, T. I. (2016). Widespread dispersal and aging of organic carbon in shallow marginal seas. *Geology* 44 (10), G37948.37941. doi: 10.1130/G37948.1

Bao, R., Uchida, M., Zhao, M., Haghipour, N., Montlucon, D. B., McNichol, A. P., et al. (2018a). Organic carbon aging during across-shelf transport. *Geophysical Res. Lett.* 45, 8425–8434. doi: 10.1029/2018GL078904

Bao, R., van der Voort, T. S., Zhao, M., Guo, X., Montluçon, D. B., McIntyre, C., et al. (2018b). Influence of hydrodynamic processes on the fate of sedimentary organic matter on continental margins. *Global Biogeochem. Cycles* 32 (9), 1420–1432. doi: 10.1029/2018gb005921

Bayona, J. M., Monjonell, A., Miquel, J. C., Fowler, S. W., and Albaigés, J. (2002). Biogeochemical characterization of particulate organic matter from a coastal hydrothermal vent zone in the Aegean Sea. *Organic Geochemistry* 33 (12), 1609–1620. doi: 10.1016/S0146-6380(02)00175-4

Bianchi, T. S., and Allison, M. A. (2009). Large-River delta-front estuaries as natural "recorders" of global environmental change. *Proc. Natl. Acad. Sci.* 106 (20), 8085–8092. doi: 10.1073/pnas.0812878106

Bianchi, T. S., Cui, X., Blair, N. E., Burdige, D. J., Eglinton, T. I., and Galy, V. (2018). Centers of organic carbon burial and oxidation at the land-ocean interface. *Organic Geochem.* 115, 138–155. doi: 10.1016/j.orggeochem.2017.09.008

Blair, N. E., and Aller, R. C. (2012). The fate of terrestrial organic carbon in the marine environment. *Annu. Rev. Mar. Sci.* 4, 401–423. doi: 10.1146/annurev-marine-120709-142717

Burdige, D. J. (2005). Burial of terrestrial organic matter in marine sediments: A re-assessment. *Global Biogeochem. Cycles* 19 (4), GB4011. doi: 10.1029/2004gb002368

Cai, A., Zhu, X., Li, Y., and Cai, Y. (1992). Sedimentary environment in Taiwan shoal. *Chin. J. Oceanol. Limnol.* 10 (4), 331–339. doi: 10.1007/BF02843834

Chen, J., Ma, J., Xu, K., Liu, Y., Cao, W., Wei, T., et al. (2016). Provenance discrimination of the clay sediment in the western Taiwan strait and its implication for coastal current variability during the late-Holocene. *Holocene* 27 (1), 110–121. doi: 10.1177/0959683616652706

Coppola, A. I., Wiedemeier, D. B., Galy, V., Haghipour, N., Hanke, U. M., Nascimento, G. S., et al. (2018). Global-scale evidence for the refractory nature of riverine black carbon. *Nat. Geosci.* 11 (8), 584–588. doi: 10.1038/s41561-018-0159-8

Dale, B. (1976). Cyst formation, sedimentation, and preservation: Factors affecting dinoflagellate assemblages in recent sediments from trondheimsfjord, Norway. *Rev. Palaeobotany Palynol.* 22 (1), 39–60. doi: 10.1016/0034-6667(76)90010-5

Eglinton, T. I., Eglinton, G., Dupont, L., Sholkovitz, E. R., Montluçon, D., and Reddy, C. M. (2002). Composition, age, and provenance of organic matter in NW African dust over the Atlantic ocean. *Geochem. Geophys. Geosystems* 3 (8), 1–27. doi: 10.1029/2001GC000269

Eglinton, G., and Hamilton, R. J. (1967). Leaf epicuticular waxes. *Science* 156 (3780), 1322–1335. doi: 10.1126/science.156.3780.1322

Feng, X., Benitez-Nelson, B. C., Montluçon, D. B., Prahl, F. G., McNichol, A. P., Xu, L., et al. (2013a). ^{14}C and ^{13}C characteristics of higher plant biomarkers in Washington margin surface sediments. *Geochimica Cosmochimica Acta* 105, 14–30. doi: 10.1016/j.gca.2012.11.034

Feng, L., Sun, J., Ning, X., Song, S., Cai, Y., and Liu, C. (2006). Phytoplankton in the northern south China Sea in summer 2004. *Oceanologia Limnologia Sin.* 37 (3), 238–248. doi: 10.3321/j.issn:0029-814X.2006.03.008

Feng, X., Vonk, J. E., van Dongen, B. E., Gustafsson, Ö., Semiletov, I. P., Dudarev, O. V., et al. (2013b). Differential mobilization of terrestrial carbon pools in Eurasian Arctic river basins. *Proc. Natl. Acad. Sci.* 110 (35), 14168–14173. doi: 10.1073/pnas.1307031110

Friedlingstein, P., Jones, M. W., O'Sullivan, M., Andrew, R. M., Hauck, J., Peters, G. P., et al. (2019). Global carbon budget 2019. *Earth System Sci. Data* 11 (4), 1783–1838. doi: 10.5194/essd-11-1783-2019

Fry, B., and Sherr, E. B. (1989). "δ13C measurements as indicators of carbon flow in marine and freshwater ecosystems," in Stable Isotopes in Ecological Research. eds. P.W. Rundel, J.R. Ehleringer and K.A. Naggy (New York: Springer), 196–229.

Galy, V., and Eglinton, T. I. (2011). Protracted storage of biospheric carbon in the Ganges-Brahmaputra basin. *Nat. Geosci.* 4 (12), 843–847. doi: 10.1016/j.palaeo.2014.09.003

Galy, V., France-Lanord, C., Beyssac, O., Faure, P., Kudrass, H., and Palhol, F. (2007). Efficient organic carbon burial in the Bengal fan sustained by the Himalayan erosional system. *Nature* 450 (7168), 407–410. doi: 10.1038/nature06273

Gao, F., Qiao, L., and Li, G. (2016). Modelling the dispersal and depositional processes of the suspended sediment in the central south yellow Sea during the winter. *Geological J.* 51 (S1), 35–48. doi: 10.1002/gj.2827

Goñi, M. A., Ruttenberg, K. C., and Eglinton, T. I. (1997). Sources and contribution of terrigenous organic carbon to surface sediments in the gulf of Mexico. *Nature* 389 (6648), 275–278. doi: 10.1038/38477

Grice, K., Klein Breteler, W. C. M., Schouten, S., Grossi, V., de Leeuw, J. W., and Damsté, J. S. S. (1998). Effects of zooplankton herbivory on biomarker proxy records. *Paleoceanography* 13 (6), 686–693. doi: 10.1029/98PA01871

Hedges, J. I., Keil, R. G., and Benner, R. (1997). What happens to terrestrial organic matter in the ocean? *Organic Geochem.* 27 (5/6), 195–212. doi: 10.1016/S0146-6380(97)00066-1

Hilton, R. G., Galy, A., Hovius, N., Chen, M. C., Horng, M. J., and Chen, H. (2008). Tropical-cyclone-driven erosion of the terrestrial biosphere from mountains. *Nat. Geosci.* 1 (2), 759–762. doi: 10.1038/ngeo333

Hilton, R. G., Galy, A., Hovius, N., Horng, M.-J., and Chen, H. (2010). The isotopic composition of particulate organic carbon in mountain rivers of Taiwan. *Geochimica Cosmochimica Acta* 74 (11), 3164–3181. doi: 10.1016/j.gca.2010.03.004

Hong, H., Zhang, C., Shang, S., Huang, B., Li, Y., Li, X., et al. (2009). Interannual variability of summer coastal upwelling in the Taiwan strait. *Continental Shelf Res.* 29 (2), 479–484. doi: 10.1016/j.csr.2008.11.007

Huh, C.-A., Chen, W., Hsu, F.-H., Su, C.-C., Chiu, J.-K., Lin, S., et al. (2011). Modern (<100 years) sedimentation in the Taiwan strait: Rates and source-to-sink pathways elucidated from radionuclides and particle size distribution. *Continental Shelf Res.* 31 (1), 47–63. doi: 10.1016/j.csr.2010.11.002

Hu, J., Kawamura, H., Hong, H., Suetsuga, M., and Lin, M. (2001). Hydrographic and satellite observations of summertime upwelling in the Taiwan strait: A preliminary description. *Terrestrial Atmospheric Oceanic Sci.* 12 (2), 415–430. doi: 10.3319/tao.2001.12.2.415(o

Kao, S.-J., Dai, M., Wei, K., Blair, N., and Lyons, W. (2008). Enhanced supply of fossil organic carbon to the Okinawa trough since the last deglaciation. *Paleoceanography* 23 (2), PA2207. doi: 10.1029/2007PA001440

Kao, S.-J., Hilton, R., Selvaraj, K., Dai, M., Zehetner, F., Huang, J.-C., et al. (2014). Preservation of terrestrial organic carbon in marine sediments offshore Taiwan: mountain building and atmospheric carbon dioxide sequestration. *Earth Surface Dynamics* 2 (1), 127–139. doi: 10.5194/esurf-2-127-2014

Kao, S. J., and Liu, K. K. (2000). Stable carbon and nitrogen isotope systematics in a human-disturbed watershed (Lanyang-hsi) in Taiwan and the estimation of biogenic particulate organic carbon and nitrogen fluxes. *Global Biogeochemical Cycles* 14 (1), 189–198. doi: 10.1029/1999GB900079

Kao, S. J., and Milliman, J. D. (2008). Water and sediment discharge from small mountainous rivers, Taiwan: the roles of lithology, episodic events, and human activities. *J. Geology* 116 (5), 431–448. doi: 10.1086/590921

Kao, S.-J., Shiah, F.-K., Wang, C.-H., and Liu, K.-K. (2006). Efficient trapping of organic carbon in sediments on the continental margin with high fluvial sediment input off southwestern Taiwan. *Continental Shelf Res.* 26 (20), 2520–2537. doi: 10.1016/j.csr.2006.07.030

Keil, R. G., Mayer, L. M., Quay, P. D., Richey, J. E., and Hedges, J. I. (1997). Loss of organic matter from riverine particles in deltas. *Geochimica Cosmochimica Acta* 61 (7), 1507–1511. doi: 10.1016/S0016-7037(97)00044-6

Keil, R. G., Tsamakis, E., Fuh, C. B., Giddings, J. C., and Hedges, J. I. (1994). Mineralogical and textural controls on the organic composition of coastal marine sediments: Hydrodynamic separation using SPLITT-fractionation. *Geochimica Cosmochimica Acta* 58 (2), 879–893. doi: 10.1016/0016-7037(94)90512-6

Komada, T., Anderson, M. R., and Dorfmeier, C. L. (2008). Carbonate removal from coastal sediments for the determination of organic carbon and its isotopic signatures, $\delta^{13}C$ and $\Delta^{14}C$: comparison of fumigation and direct acidification by hydrochloric acid. *Limnology Oceanography* 6, 254–262. doi: 10.4319/lom.2008.6.254

Lan, K. W., Lee, M. A., Zhang, C. I., Wang, P. Y., Wu, L. J., and Lee, K. T. (2014). Effects of climate variability and climate change on the fishing conditions for grey mullet (mugil cephalus l.) in the Taiwan strait. *Climatic Change* 126 (1-2), 189–202. doi: 10.1007/s10584-014-1208-y

Lan, K.-W., Lian, L.-J., Li, C.-H., Hsiao, P.-Y., and Cheng, S.-Y. (2020). Validation of a primary production algorithm of vertically generalized production model derived from multi-satellite data around the waters of Taiwan. *Remote Sens.* 12 (10), 1627. doi: 10.3390/rs12101627

Lan, K. W., Zhang, C. I., Kang, H. J., Wu, L. J., and Lian, L. J. (2017). Impact of fishing exploitation and climate change on the grey mullet mugil cephalus stock in the Taiwan strait. *Mar. Coast. Fisheries* 9 (1), 271–280. doi: 10.1080/19425120.2017.1317680

Lee, J., Liu, J. T., Hung, C.-C., Lin, S., and Du, X. (2016). River plume induced variability of suspended particle characteristics. *Mar. Geology* 380, 219–230. doi: 10.1016/j.margeo.2016.04.014

Liao, W., Hu, J., and Peng, P.a. (2018). Burial of organic carbon in the Taiwan strait. *J. Geophysical Research: Oceans* 123 (9), 6639–6652. doi: 10.1029/2018jc014285

Liu, J. T., Hsu, R. T., Yang, R. J., Wang, Y. P., Wu, H., Du, X., et al. (2018). A comprehensive sediment dynamics study of a major mud belt system on the inner shelf along an energetic coast. *Sci. Rep.* 8, 4229. doi: 10.1038/s41598-018-22696-w

Liu, J. T., Huang, B., Chang, Y., Du, X., Liu, X., Yang, R. J., et al. (2019). Three-dimensional coupling between size-fractionated chlorophyll-a, POC and physical processes in the Taiwan strait in summer. *Prog. Oceanogr.* 176, 102129. doi: 10.1016/j.pocean.2019.102129

Liu, J. T., Kao, S. J., Huh, C. A., and Hung, C. C. (2013). Gravity flows associated with flood events and carbon burial: Taiwan as instructional source area. *Annu. Rev. Mar. Sci.* 5 (5), 47–68. doi: 10.1146/annurev-marine-121211-172307

Liu, J. T., Lee, J., Yang, R. J., Du, X., Li, A., Lin, Y.-S., et al. (2021a). Coupling between physical processes and biogeochemistry of suspended particles over the inner shelf mud in the East China Sea. *Mar. Geology* 442, 106657. doi: 10.1016/j.margeo.2021.106657

Liu, J. P., Liu, C. S., Xu, K. H., Milliman, J. D., Chiu, J. K., Kao, S. J., et al. (2008). Flux and fate of small mountainous rivers derived sediments into the Taiwan strait. *Mar. Geology* 256 (1–4), 65–76. doi: 10.1016/j.margeo.2008.09.007

Liu, M., Zheng, J., Krock, B., Ding, G., MacKenzie, L., Smith, K. F., et al. (2021b). Dynamics of the toxic dinoflagellate *alexandrium pacificum* in the Taiwan strait and its linkages to surrounding populations. *Water* 13, 2681. doi: 10.3390/w13192681

Li, D., Zhao, M., and Chen, M. T. (2014). East Asian Winter monsoon controlling phytoplankton productivity and community structure changes in the southeastern south China Sea over the last 185kyr. *Palaeogeogr. Palaeoclimatol. Palaeoecol.* 417 (414), 576–576. doi: 10.1016/j.palaeo.2014.09.003

Mayer, L. M. (1994). Surface area control of organic carbon accumulation in continental shelf sediments. *Geochimica Cosmochimica Acta* 58 (4), 1271–1284. doi: 10.1016/0016-7037(94)90381-6

McDuffee, K. E., Eglinton, T. I., Sessions, A. L., Sylva, S., Wagner, T., and Hayes, J. M. (2004). Rapid analysis of ^{13}C in plant-wax n-alkanes for reconstruction of terrestrial vegetation signals from aquatic sediments. *Geochemistry Geophysics Geosystems* 5 (10), Q10004. doi: 10.1029/2004GC000772

Mei, X., Meng, X., Wang, Z., Wang, Z., and Nan, Q. (2019). Abundance and community structure of the phytoplankton in surface sediments recorded by biomarkers from liaodong bay. *Mar. Geology Front.* 35 (2), 10–17. doi: 10.16028/j.1009-2722.2019.02002

Milliman, J.D., and Farnsworth, K.L. (2011). "Runoff, erosion, and delivery to the coastal ocean," in River Discharge to the Coastal Ocean: *A Global Synthesis*. (Cambridge: Cambridge University Press), 13–69. doi: 10.1017/CBO9780511781247.003

Milliman, J. D., and Farnsworth, K. L. (2013). "River discharge to the coastal ocean," in *A global synthesis* (New York: Cambridge University Press).

Regnier, P., Resplandy, L., Najjar, R. G., and Ciais, P. (2022). The land-to-ocean loops of the global carbon cycle. *Nature* 603 (7901), 401–410. doi: 10.1038/s41586-021-04339-9

Resio, D. T., and Hayden, B. P. (1975). Recent secular variations in mid-Atlantic winter extratropical storm climate. *J. Appl. Meteorol. Clim.* 14 (7), 1223–1234. doi: 10.1175/1520-0450(1975)014<1223:RSVIMA>2.0.CO;2

Rommerskirchen, F., Eglinton, G., Dupont, L., and Rullkötter, J. (2006). Glacial/interglacial changes in southern Africa: Compound-specific $\delta^{13}C$ land plant biomarker and pollen records from southeast Atlantic continental margin sediments. *Geochem. Geophys. Geosystems* 7 (8), Q08010. doi: 10.1029/2005gc001223

Tao, S., Eglinton, T. I., Montluçon, D. B., McIntyre, C., and Zhao, M. (2015). Pre-aged soil organic carbon as a major component of the yellow river suspended load: Regional significance and global relevance. *Earth Planetary Sci. Lett.* 414 (0), 77–86. doi: 10.1016/j.epsl.2015.01.004

Tao, S., Eglinton, T. I., Montluçon, D. B., McIntyre, C., and Zhao, M. (2016). Diverse origins and pre-depositional histories of organic matter in contemporary Chinese marginal sea sediments. *Geochimica Cosmochimica Acta* 191, 70–88. doi: 10.1016/j.gca.2016.07.019

Tseng, H.-C., You, W.-L., Huang, W., Chung, C.-C., Tsai, A.-Y., Chen, T.-Y., et al. (2020). Seasonal variations of marine environment and primary production in the Taiwan strait. *Front. Mar. Sci.* 7. doi: 10.3389/fmars.2020.00038

Walsh, J. P., and Nittrouer, C. A. (2009). Understanding fine-grained river-sediment dispersal on continental margins. *Mar. Geology* 263 (1), 34–45. doi: 10.1016/j.margeo.2009.03.016

Wang, Y. H., Jan, S., and Wang, D. P. (2003). Transports and tidal current estimates in Taiwan strait from shipboard ADCP observation (1999-2001). *Estuar. Coast. Shelf Sci.* 57 (1–2), 193–199. doi: 10.1016/S0272-7714(02)00344-X

Wang, A., Ye, X., Liu, J. T., Xu, Y. H., Yin, X. J., and Xu, X. H. (2017). Sources of settling particulate organic carbon during summer in the northern Taiwan strait. *Estuar. Coast. Shelf Sci.* 198, 487–496. doi: 10.1016/j.ecss.2016.10.008

Wang, A., Ye, X., Xu, X., Yin, X., and Xu, Y. (2018). Settling flux and origin of particulate organic carbon in a macro-tidal semi-enclosed embayment: Luoyuan bay, southeast China coast. *Estuar. Coast. Shelf Sci.* 206, 38–48. doi: 10.1016/j.ecss.2017.03.023

Weijers, J. W. H., Schouten, S., Schefuß, E., Schneider, R. R., and Sinninghe Damsté, J. S. (2009). Disentangling marine, soil and plant organic carbon contributions to continental margin sediments: A multi-proxy approach in a 20,000 year sediment record from the Congo deep-sea fan. *Geochimica Cosmochimica Acta* 73 (1), 119–132. doi: 10.1016/j.gca.2008.10.016

Wu, G., Cao, W., Huang, Z., Kao, C.-M., Chang, C.-T., Chiang, P.-C., et al. (2017). Decadal changes in nutrient fluxes and environmental effects in the jiulong river estuary. *Mar. pollut. Bull.* 124 (2), 871–877. doi: 10.1016/j.marpolbul.2017.01.071

Wu, Y., Eglinton, T., Yang, L., Deng, B., Montluçon, D., and Zhang, J. (2013). Spatial variability in the abundance, composition, and age of organic matter in surficial sediments of the East China Sea. *J. Geophysical Research: Biogeosciences* 118 (4), 1495–1507. doi: 10.1002/2013JG002286

Xing, L., Tao, S., Zhang, H., Liu, Y., Yu, Z., and Zhao, M. (2011). Distributions and origins of lipid biomarkers in surface sediments from the southern yellow Sea. *Appl. Geochem.* 26 (8), 1584–1593. doi: 10.1016/j.apgeochem.2011.06.024

Xing, L., Zhao, M., Gao, W., Wang, F., Zhang, H., Li, L., et al. (2014). Multiple proxy estimates of source and spatial variation in organic matter in surface sediments from the southern yellow Sea. *Organic Geochemistry* 76, 72–81. doi: 10.1016/j.orggeochem.2014.07.005

Xu, K., Li, A., Liu, J. P., Milliman, J. D., Yang, Z., Liu, C.-S., et al. (2012). Provenance, structure, and formation of the mud wedge along inner continental shelf of the East China Sea: A synthesis of the Yangtze dispersal system. *Mar. Geology* 291–294 (0), 176–191. doi: 10.1016/j.margeo.2011.06.003

Xu, K., Milliman, J. D., Li, A., Paul Liu, J., Kao, S.-J., and Wan, S. (2009). Yangtze- and Taiwan-derived sediments on the inner shelf of East China Sea. *Continental Shelf Res.* 29 (18), 2240–2256. doi: 10.1016/j.csr.2009.08.017

Yamaguchi, M., Itakura, S., Nagasaki, K., and Kotani, Y. (2002). Distribution and abundance of resting cysts of the toxic alexandrium spp. (Dinophyceae) in sediments of the western seto inland Sea, Japan. *Fisheries Sci.* 68 (5), 1012–1019. doi: 10.1046/j.1444-2906.2002.00526.x

Yang, R. J., Liu, J. T., Su, C.-C., Chang, Y., Xu, J. J., and Lui, H.-K. (2021). Land-ocean interaction affected by the monsoon regime change in Western Taiwan strait. *Front. Mar. Sci.* 8. doi: 10.3389/fmars.2021.735242

Zhang, G., Liang, S., Shi, X., and Han, X. (2015). Dissolved organic nitrogen bioavailability indicated by amino acids during a diatom to dinoflagellate bloom succession in the changjiang river estuary and its adjacent shelf. *Mar. Chem.* 176, 83–95. doi: 10.1016/j.marchem.2015.08.001

Zhao, B., Yao, P., Bianchi, T. S., and Yu, Z. G. (2021). Controls on organic carbon burial in the Eastern China marginal seas: A regional synthesis. *Global Biogeochem. Cycles* 35 (4), e2020GB006608. doi: 10.1029/2020GB006608

Zheng, L.-W., Ding, X., Liu, J. T., Li, D., Lee, T.-Y., Zheng, X., et al. (2017). Isotopic evidence for the influence of typhoons and submarine canyons on the sourcing and transport behavior of biospheric organic carbon to the deep sea. *Earth Planetary Sci. Lett.* 465, 103–111. doi: 10.1016/j.epsl.2017.02.037

Zhou, Q., Chen, C., Liang, J., and Gao, Y. (2015b). Species composition and seasonal variation of netz-phytoplankton in the eastern marginal China seas. *Biodiversity Sci.* 23 (1), 23–32. doi: 10.17520/biods.2014103

Zhou, C., Dong, P., and Li, G. (2015a). Hydrodynamic processes and their impacts on the mud deposit in the southern yellow Sea. *Mar. Geol.* 360, 1–16. doi: 10.1016/j.margeo.2014.11.012

Zhu, C., Wang, Z.-H., Xue, B., Yu, P.-S., Pan, J.-M., Wagner, T., et al. (2011a). Characterizing the depositional settings for sedimentary organic matter distributions in the lower Yangtze river-East China Sea shelf system. *Estuarine Coast. Shelf Sci.* 93 (3), 182–191. doi: 10.1016/j.ecss.2010.08.001

Zhu, C., Weijers, J. W., Wagner, T., Pan, J.-M., Chen, J.-F., and Pancost, R. D. (2011b). Sources and distributions of tetraether lipids in surface sediments across a large river-dominated continental margin. *Organic Geochem.* 42 (4), 376–386. doi: 10.1016/j.orggeochem.2011.02.002